ELSEVIER

Surface Science 327 (1995) 165-191

surface science

He scattering from compact clusters and from diffusion-limited aggregates on surfaces: observable signatures of structure

D.A. Hamburger[a,b], A.T. Yinnon[b], I. Farbman[b], A. Ben-Shaul[b], R.B. Gerber[b,c,*]

[a] *Department of Physics, The Racah Institute, The Hebrew University of Jerusalem, Jerusalem 91904, Israel*

[b] *Department of Physical Chemistry and The Fritz Haber Center for Molecular Dynamics, The Hebrew University of Jerusalem, Jerusalem 91904, Israel*

[c] *Department of Chemistry, University of California, Irvine, CA 92717, USA*

Received 6 April 1994; accepted for publication 5 December 1994

Abstract

The angular intensity distribution of He beams scattered from compact clusters and from diffusion limited aggregates, epitaxially grown on metal surfaces, is investigated theoretically. The purpose is two-fold: to distinguish compact cluster structures from diffusion limited aggregates, and to find observable *signatures* that can characterize the compact clusters at the atomic level of detail. To simplify the collision dynamics, the study is carried out in the framework of the sudden approximation, which assumes that momentum changes perpendicular to the surface are large compared with momentum transfer due to surface corrugation. The diffusion limited aggregates on which the scattering calculations were done, were generated by kinetic Monte Carlo simulations. It is demonstrated, by focusing on the example of compact Pt heptamers, that signatures of structure of compact clusters may indeed be extracted from the scattering distribution. These signatures enable both an experimental distinction between diffusion limited aggregates and compact clusters, and a determination of the cluster structure. The characteristics comprising the signatures are, to varying degrees, the rainbow, Fraunhofer, specular and constructive interference peaks, all seen in the intensity distribution. It is also shown, how the distribution of adsorbate heights above the metal surface can be obtained by an analysis of the specular peak attenuation. The results contribute to establishing He scattering as a powerful tool in the investigation of surface disorder and epitaxial growth on surfaces, alongside with STM.

Keywords: Atom–solid interactions, scattering, diffraction; Clusters; Dendritic and/or fractile surfaces; Epitaxy; Metal–metal nonmagnetic thin film structures; Platinum; Surface defects; Surface structure

1. Introduction

The process of epitaxial growth of metal or semiconductor films on a surface presents some major theoretical, experimental and technological challenges. In epitaxial growth, metal or semiconductor atoms are adsorbed on a corresponding surface under thermal conditions, to form two- and three-dimensional structures on top of it.

* Corresponding author.

SSDI 0039-6028(94)00828-0

The physical and chemical properties are determined by the final form of these structures. These may be of dramatic importance, e.g. in the production of electronic devices. One of the most exciting aspects of epitaxial growth kinetics, is that it *prepares disordered structures* in the intermediate stages. The disorder manifests itself in the formation of various types of clusters or diffusion-limited-aggregates (DLA) on top of the surface. These structures may be monolayers (usually at high temperatures, when the diffusivity is large), in which case the disorder is two-dimensional, or they may be composed of several layers, giving rise to disorder in three dimensions. Epitaxially grown structures of this type have for some time now received wide attention, as they offer an exceptional opportunity for both experimental and theoretical study of disorder. Clusters in particular play an important role in the epitaxial-growth kinetics, as it is the continual process of their formation, restructuring and dissociation, through which growth actually takes place. Issues such as the structure, stability and surface diffusion of metal clusters have been addressed experimentally by Wang and Ehrlich [1]. Rosenfeld et al. [2] have recently suggested the intriguing possibility of the formation over a certain temperature and coverage range, of a high density of small, stable and compact clusters of seven ad-atoms of Pt (heptamers), during the process of epitaxial growth of Pt on Pt(111). A recent theoretical first-principles study by Stumpf and Scheffler [3] predicts hexagonally shaped islands for Al on Al(111). These developments tentatively suggest that metastable states of systems consisting of clusters of well-defined shape, and perhaps size may exist. Regarding DLA, several authors [4–7] have presented simulations which reveal the complexity anticipated in the shapes of these structures, in which no regular clusters can be discerned. As these and other studies show, a large variety of structures contribute to surface disorder. No satisfactory and comprehensive theory of the epitaxial growth process is as of yet available, much due to the absence of reliable interaction potentials between the ad-atoms and the surface. Progress at this stage thus hinges critically on experiments. To a large extent the information obtained from different modern methods is complementary. Since the various techniques probe different aspects and distance scales of the surface structures, the most comprehensive picture will probably be attained via an integration of results from all techniques. TEAS and in particular He-beams, has already proved among the most useful tools in analyzing surface phenomena. Experiments by Poelsema and co-workers [8–11] and Ernst and coworkers [12–15] have employed He-scattering in dealing with questions concerned with scattering from isolated surface defects, and were so able to extract a wealth of information on the defects and their mutual attractions. The attenuation of specular intensities, in particular, proves an extremely useful tool in these investigations. Theoretical studies by Gerber and co-workers [16–19] utilizing both time independent (sudden approximation) and time-dependent methods (quantum wave-packets), have analyzed the calculated angular distribution and specular peak attenuation. These authors have been able to identify connections between the features of the distribution and the attenuation, and microscopic characteristics related to the surface defects. An important advantage offered by He-scattering, is that He is capable of probing structure both at the *local* and *global* levels. The interpretation of He-scattering experiments, however, is rather more involved than that of the direct-imaging techniques such as FIM and STM. The purpose of the present article is to address the questions of whether "signatures" of the various shapes assumed by the clusters and DLA are present in the spectra obtained with He-scattering experiments, and to find how they may be extracted with the proper analysis. The answers to these questions are crucial to the understanding of epitaxial-growth induced surface disorder, and to enhance the usefulness of TEAS as an indispensable tool in the study of such surface phenomena. The experiments by Rosenfeld et al. [2] and Bott et al. [20] on Pt and by Ehrlich et al. [1] on Ir suggest that under proper conditions compact clusters may be observed as a dominant phase, whereas DLA will predominate under other conditions [20]. This is supported by Stumpf and Scheffler's theoretical calculations for Al [3]. It will be our main purpose in this article to demonstrate that compact clusters can easily be distinguished from DLA in a He-scattering experiment. Furthermore we hope to demonstrate, using the example of compact heptamers as a case study for clusters, that specific structure-related characteristics of compact clusters can indeed be extracted from an analysis of the angular intensity distribution, and that these characteristics, when combined, provide an almost unique signature of the structure. Thus by a detailed examination of the angular intensity distribution calculated from several model systems, we seek to show that surface-adsorbed structures

exhibiting various types of disorder, can be *characterized* by means of He-scattering experiments. The structure of the article is as follows: In Section 2 we discuss our model systems. Section 3 briefly discusses the methods employed for studying the scattering intensities. Section 4 describes the results of scattering calculations from our model systems. Concluding remarks are brought in Section 5.

2. The model systems

The present study deals with the scattering of a He beam from various types of disordered structures, considered pertinent to epitaxial growth modes. The possible formation of such structures in kinetic simulations of growth is also treated briefly. We shall treat two types of structures:

(i) *Compact clusters on a surface*
Within this family, disorder will be represented in an increasing degree of complexity, by considering three related models:
(a) A single heptamer on an otherwise completely flat Pt(111) surface.
(b) A collection of heptamers on the same Pt surface, adsorbed at random positions, but having orientations compatible with the underlying hexagonal symmetry.
(c) A collection of heptamers on the same Pt surface, adsorbed both at random positions and with random orientations in the surface plane.

(ii) *Diffusion limited aggregates on a surface.*
Here we considered non-compact structures, grown under kinetic conditions.

The clusters and the underlying surface were treated as a static, nonvibrating target in the scattering calculations. Clearly, vibrations of the adsorbate atoms and the surface are expected to affect quantitatively the scattering distributions measured in TEAS experiments. However, results of calculations using a rigid, nonvibrating surface system should be useful at least for studying the main qualitative effects. Moreover, for diffraction scattering from crystalline surfaces, the effect of surface vibrations on the scattering intensities can be represented approximately by a simple Debye–Waller factor [21]. A similar description is expected to be successful also for the scattering intensities from clusters on surfaces. In the context of studies of the specular attenuation, work by Poelsema and coworkers [22] has demonstrated that treating the surface as static is a very useful approximation in analyzing specular scattering from disordered surfaces. The Pt surface in the scattering calculations reported here was treated as completely flat. For a very low corrugation surface such as Pt(111), this should be a good approximation. We now describe in some detail the three models of compact heptamer clusters and the model of kinetic growth of DLA on the surface, all of which were used for the scattering calculations.

2.1. Single heptamer on a flat Pt surface

In this section we describe a model for a single, symmetric and static heptamer on a smooth metal surface. The parameters were chosen to represent a Pt heptamer on a Pt(111) surface. Although we do not expect a TEAS experiment to ever probe a surface with just a single heptamer adsorbed upon it, the study of the angular intensity distribution produced by such an arrangement is crucial in understanding the specific heptamer related features. As a motivation for our choice of potential, consider the role of the conduction electrons. Clearly the heptamer is immersed in the sea of surface conduction electrons. However, we expect the surface to be much smoother than the heptamer's top, due to a flow of electrons from the top to the surface. The extent to which the heptamer's nuclei lie bare determines both the heptamer's height above the surface and its top's corrugation. These are very important parameters in determining the scattering features. A simple, albeit inexact, class of potentials which satisfy the requirement of a corrugated heptamer-top, are those which are pairwise additive in the top. We assume the heptamer to be composed of an isolated cluster of seven Pt atoms adsorbed on a flat Pt

surface, with six Pt atoms forming a perfect hexagon and the seventh atom located at its center. The interaction between the gas phase He and the Pt surface with its adsorbed cluster is assumed additive and is represented by the following potential function:

$$V(\boldsymbol{r}) = V_s(z) + \sum_{i=1}^{7} V_{\text{He-Pt}}(|\boldsymbol{r} - \boldsymbol{r}_i|), \tag{1}$$

where $\boldsymbol{r} = (x, y, z)$, $V_s(z)$ represents the interaction between He and a flat Pt(111) surface, and $V_{\text{He-Pt}}(|\boldsymbol{r} - \boldsymbol{r}_i|)$ represents the interaction between He and the ith Pt atom in the cluster, located at $\boldsymbol{r}_i$. The coordinate z measures the distance of the He atom from the surface plane, while (x, y) are the coordinates in parallel to the surface plane. The functional form of $V_s(z)$ was chosen as:

$$V_s(z) = D_s \left(\frac{{z_m}^9}{z^9} - \frac{3\,{z_m}^3}{z^3} \right) \tag{2}$$

which is a surface scattering version of a Lennard-Jones 6–12 potential. The value $D_s = 4.0$ meV ($= 8.464 \times 10^{-5}$ a.u.), given by Harris et al. [23] was employed, and z_m was taken as 7.87 a.u., which gives a steepness typical of atom–atom interactions with metal surfaces. For $V_{\text{He-Pt}}$ a Lennard-Jones 6–12 potential was used:

$$V_{\text{He-Pt}}(r) = \frac{c_{12}}{r^{12}} - \frac{c_6}{r^6}. \tag{3}$$

We assumed that the c_6 interaction parameter between He and a heavy atom X scales linearly with the polarizability of X. The polarizability, in turn, was estimated from the available atomic volume. In our estimate, the c_6 parameter so obtained is sufficiently reliable for the qualitative purposes of this paper. Thus:

$$c_6(\text{Pt–He}) \sim c_6(\text{Xe–He}) \times \text{Vol(Pt)}/\text{Vol(Xe)} = 6.322 \text{ a.u.}$$

The c_{12} parameter was extracted from Eq. (2) by the formula:

$$V_s(z) = \frac{1}{S^{\frac{3}{2}}} 2\pi \int_z^\infty \mathrm{d}r \left(r^2 - r\,z\right) V_{\text{He-Pt}}(r), \tag{4}$$

where S is the unit-cell area. This equation is based on taking the continuum limit of a sum of pairwise He/Pt interactions. It gives a value of $c_{12} = 3.251 \times 10^7$ a.u. We do not have ab-initio calculations available to provide reliable estimates of our additive-potentials model, and thus we do not expect the interaction potential Eq. (1) to be quantitatively correct, but we expect this potential to be realistic on a semiquantitative footing. This should suffice for the purpose of searching for qualitative effects in the angular distribution.

2.2. *Randomly adsorbed heptamers*

The situation we expect to find in a real experiment is a *distribution* of clusters of various sizes and shapes: isolated heptamers are probably not realized at the coverages of interest for epitaxial growth. Consider as a conjecture the existence of heptamer cluster phases. If confirmed after further study, this distribution will exhibit a pronounced peak for symmetrical heptamers. Hence a more realistic treatment of the scattering off heptamers must involve a distribution of heptamers on a surface. The heptameric-phase conjecture does, however, leave us with a freedom to consider two models of a distribution of adsorbed heptamers. These correspond to different degrees of disorder, and follow from the possibility of either a high or low barrier for rotation of a heptamer-cluster as a whole, as explained below. In this section we investigate the scattering from the two corresponding distributions of heptamers, while ignoring the possible existence of other cluster types. We expect the other

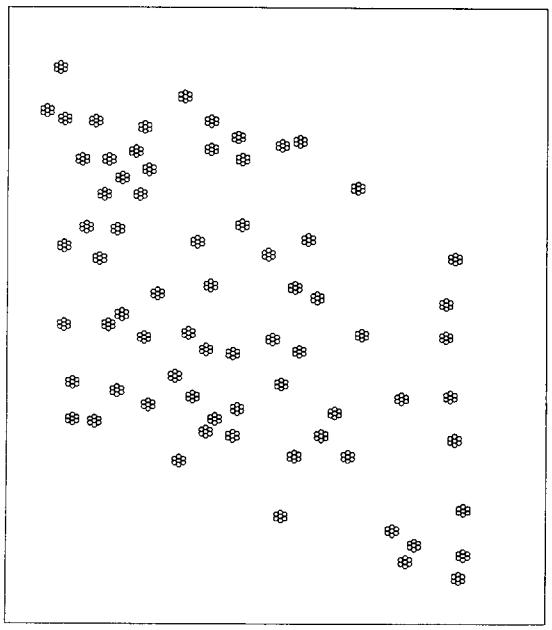

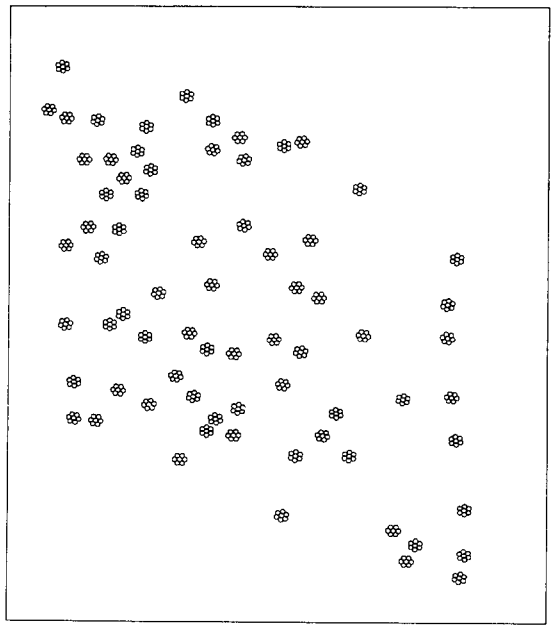

Fig. 1. (Left) Schematic representation of translationally random heptamers at 5% coverage on Pt(111). Although the heptamers occupy random lattice sites, they clearly have orientations compatible with the underlying hexagonal symmetry of the surface.

Fig. 2. (Right) Translationally and rotationally random heptamers at 5% coverage on Pt(111). Here the heptamers do not obey an orientational constraint. Instead their orientation is picked at random from a uniform distribution. Their centers of mass occupy random lattice sites.

cluster types not to alter the central features of the intensity spectrum, provided the distribution is peaked sharply enough about the heptamers. In this sense the present framework is an adequate tool for our purpose of providing signatures of heptamers. In the two models we investigated in this section we considered the case of randomly adsorbed heptamers. In both, the center of each heptamer was chosen randomly from a uniform distribution, and then placed on the nearest lattice site. We excluded those heptamers that overlapped with or bordered on other heptamers, i.e., those where the distance of Pt atoms belonging to two different clusters was less than two unit cells apart. We distinguish between two possibilities:

2.2.1. Translationally random heptamers on Pt(111)

Since it is plausible that the orientation of the heptamers is determined by the surface structure, we located each cluster Pt atom at the center of the triangles that make up the underlying hexagonal structure of the surface Pt atoms (i.e., a lattice site). This corresponds to a high barrier for rotation of a heptamer-cluster as a whole. It leads to a six-fold symmetry in the orientations of the heptamers. Part of the surface is shown in Fig. 1.

2.2.2. Translationally and rotationally random heptamers on Pt(111)

Though the surface-induced orientation described in Section 2.2.1 seems intuitively physically correct, we cannot exclude a completely randomly distributed orientation of the heptamers, corresponding to a low barrier for rotation of a heptamer-cluster as a whole. Therefore we investigated a second model, where also the orientation of the heptamers is chosen randomly from a uniform distribution, as can be seen in Fig. 2. For both cases the coverage of the adsorbed Pt atoms was 5% of a monolayer. The He/Pt cluster+surface interaction

for these models is given by Eq. (1), with the exception of the second term which now contains an additional sum over all N heptamers:

$$V(\boldsymbol{r}) = \sum_{n=1}^{N} \sum_{i=1}^{7} V_{\mathrm{He\text{-}Pt}}(|\boldsymbol{r} - \boldsymbol{r}_{i,n}|) + V_{\mathrm{s}}(z). \tag{5}$$

Here $\boldsymbol{r}_{i,n} = (x_{i,n}, y_{i,n}, z_{i,n})$ represents the location of the ith Pt atom in the nth heptamer.

2.3. *Diffusion limited aggregates grown by kinetic Monte Carlo (KMC)*

We now proceed to consider not only compact clusters, but structures that can develop in kinetic conditions. The main factors determining the shapes of the resulting structures are:

(i) The deposition rate of the Pt atoms,

(ii) Spatial migration of the Pt atoms upon the surface.

There is an extensive literature dealing with the modeling of the process of diffusion and aggregation upon a homogeneous surface [24]. The approach that will be taken here to simulate the time-dependent structures obtained in the course of deposition and migration, is the KMC scheme [25]. The essence of the approach is assigning probabilities for the hopping of adsorbed atoms between allowed sites upon the surface, which is assumed a lattice. To obtain probabilities for hops between the different configurations, assumptions about energetics and interactions must be made. We shall present a kinetic model for growth of monolayer Pt islands on a flat Pt surface. Our purpose in examining this model was to provide realistic adsorbate structures for the He-scattering calculations. This enabled us to investigate possible ways of discriminating between these structures and formations of heptamers. In order to produce realistic arrangements of adatoms on the surface we performed kinetic Monte Carlo (KMC) simulations, using a model of pairwise additive interactions and a time dependent Monte Carlo (TDMC) procedure. The simulation took place on a hexagonal lattice of 100×100 unit cells with periodic boundary conditions. The simulation starts with two particles on the surface diffusing until a third particle adsorbs. This period is typically 0.05 s (for simulating an adsorption rate of 500 s/ML [2]) corresponding to about 10^6 MC steps at room temperature. Then the three particles diffuse, a fourth one adsorbs, and so on until 500 particles, corresponding to 5% coverage, diffuse on the surface for 0.05 s. The configurations attained are not at equilibrium.

The interactions model: The simulations were performed using two different kinetic models for lateral interactions between the adsorbed particles. In the first model, every particle was assigned an energy according to the number of its nearest neighbors

$$E(n) = E_0 + n\epsilon, \tag{6}$$

where E_0 is the activation energy for diffusion at zero coverage, n is the number of nearest neighbors and ϵ is the nearest neighbor interaction energy. Particle diffusion takes place via random walks between nearest neighbor sites. The hopping rate (transition probability per unit time) of a particle from site i, where it has n_{i} nearest neighbors, to a neighboring site with n_{f} nearest neighbors, is taken as

$$\omega_{\mathrm{i}\to\mathrm{f}} = \nu\, \mathrm{e}^{-E(n_{\mathrm{i}})/kT} = \omega_0\, \mathrm{e}^{-n_{\mathrm{i}}\epsilon/kT}, \tag{7}$$

where $\omega_0 = \nu \exp[-E_0/(kT)]$ is the hopping frequency of an "isolated" particle. $\tau_0 = 1/\omega_0$, the average time interval between successive moves on the bare (zero coverage) surface, sets the unit of time for simulations performed at a given temperature T. Clearly, $\omega_{\mathrm{i}\to\mathrm{f}}$ satisfies detailed balance, since $\omega_{\mathrm{i}\to\mathrm{f}}/\omega_{\mathrm{f}\to\mathrm{i}} = \exp[-(E_{\mathrm{f}} - E_{\mathrm{i}})/(kT)]$ with $E_{\mathrm{i}} = E(n_{\mathrm{i}})$ and $E_{\mathrm{f}} = E(n_{\mathrm{f}})$. Note that according to Eq. (7), the transition rate depends only on the initial state. A possible dynamical interpretation of this model, originally suggested by Uebing and Gomer

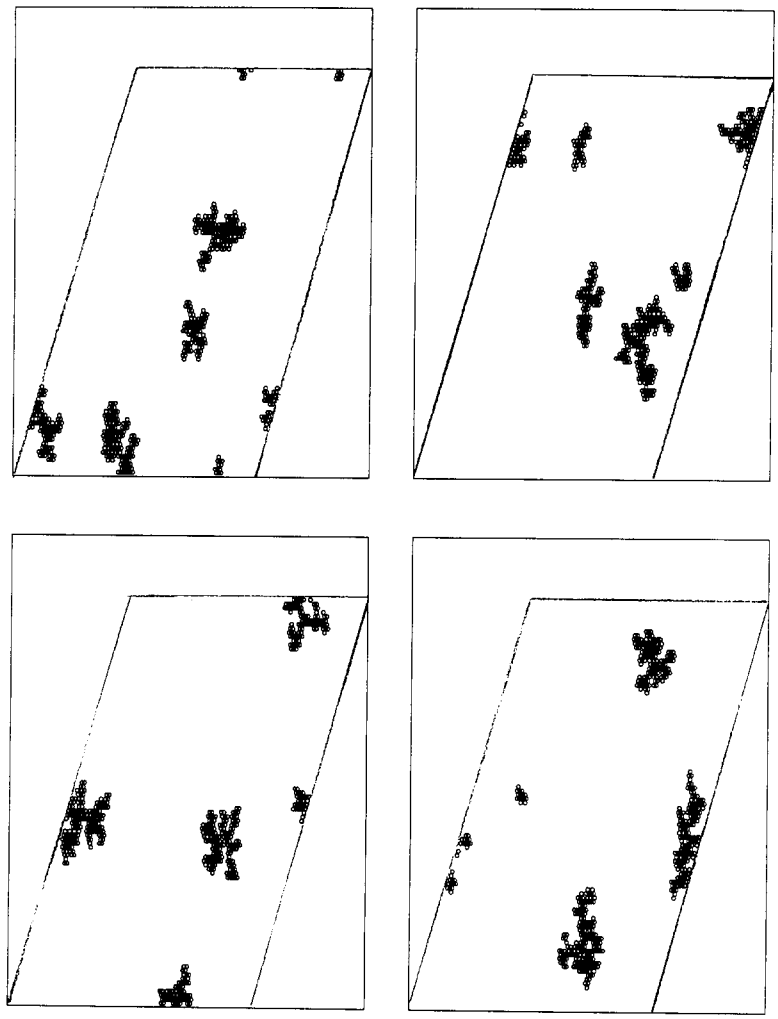

Fig. 3. Pt islands produced by KMC simulations, at 5% coverage on surfaces of 100 × 100 unit cells, according to the model with energy independent of cluster size (first model; see text). The surface is a parallelogram with an angle of 60°. Periodic boundary conditions are employed, so straight edges usually imply that the cluster is continued at the opposite boundary. The configurations displayed differ only in the random number sequences used to generate them.

[26], is that the rate of the transition from state i to state f, is governed by the rate at which the particle in state i escapes into a transition state (saddle point) which is the same for all possible transitions into different final states. Examples of structures produced by this model are shown in Fig. 3.

In the second model we continued to use Eq. (7) for the transition rates, but now instead of Eq. (6), the energy of a particle in a given configuration is:

$$E(n,s) = E_0 + n\epsilon(s), \tag{8}$$

with n denoting, as before, the number of nearest neighbors of the particle under consideration, and s being the size of the cluster the particle belongs to. According to this model, the nearest neighbor interaction energy $\epsilon(s)$, depends on the cluster size (thus, indirectly, taking into account the effects of non-additive interactions). The

assumption on the nature of the interaction is critical. It is clear that by assuming certain types of dependence of the microcluster energy upon shape and size, one can ultimately obtain any chosen type of kinetic behavior and global structure. We believe that the dependences we used, while definitely not quantitatively valid, represent at least a qualitative plausible energetic behavior of a system of this type. The values of $\epsilon(s)$ (for Pt atoms on Pt(111)) were taken from the work of Rosenfeld et al. [27], who used Eq. (8) in their rate equation study of Pt diffusion and aggregation. More specifically, these authors used: $\epsilon(s) = \epsilon(2) - (s-2)\,\Delta\epsilon$, with $\epsilon(2) = 0.300$ eV, and $\Delta\epsilon = 0.015$ eV for $2 \leq s \leq 6$, and: $\epsilon(s) = \epsilon(6) - (s-6)\,\Delta\epsilon$, with $\epsilon(6) = 0.240$ eV, and $\Delta\epsilon = 0.005$ eV for $7 \leq s \leq 14$. Using this model in their rate equation approach, Rosenfeld et al. find a strong tendency for heptamer formation at $T \geq 400$ K. On the other hand, our KMC simulations, using the same model for $\epsilon(s)$, did not reveal a particular preference for *heptamer* formation: mostly larger compact clusters were produced, with the number of constituent atoms varying from cluster to cluster. The difference must be attributed to the mean field type approximations inherent to the rate equation formalism. Having no reliable kinetic means at our disposal to produce compact heptameric islands, we used only the simpler first model to provide realistic adsorbate structures for our scattering calculations. The KMC simulations (for both models) were performed using the time-dependent Monte-Carlo (TDMC) scheme, suggested in Ref. [25]. According to this scheme, instead of randomly choosing particles and accepting or rejecting moves according to the given transition probabilities (as in "traditional" MC simulations), one performs a move in any attempt, and propagates the time accordingly. More explicitly, we first calculate the average transition rate $\langle r \rangle = 1/\langle \omega_{i\to f} \rangle$ out of state i, then randomly sample a given $i \to f$ move with probability $\omega_{i\to f}/\sum \omega_{i\to f}$ and, finally, perform this move and record the time elapsed as $\Delta t = 1/\langle r \rangle$. Further details about this procedure can be found elsewhere [24,25].

2.4. Interaction potential of He with DLA structures

We proceeded to perform scattering calculations from the DLA structures. Our purpose here was to check the degree of specificity of the features exhibited by the angular intensity distribution obtained from the heptamer systems of Sections 2.2.1 and 2.2.2. The results of the KMC grown structures are the best model system we had at hand to simulate a non-heptameric epitaxial surface. This model served as our control-case, against which the features identified for the heptameric models were tested. We will consider more fully the question of what structural features can be extracted from the information contained in the scattering results from the DLA structures in a future article. The potential used for the He scattering calculations in this case was:

$$V(\boldsymbol{r}) = V_s(z) + \sum_{i=1}^{N} V_{\text{He-Pt}}(|\boldsymbol{r} - \boldsymbol{r}_i|), \tag{9}$$

where $V_s(z)$ and $V_{\text{He-Pt}}$ are given by Eqs. (2) and (3), respectively, and $\boldsymbol{r}_i$ now runs over the positions of all adsorbed Pt atoms.

3. The methods for the scattering calculations

We employed the sudden approximation [28–32], which has proved very useful in studies of atom scattering from defects. Basically, the sudden approximation requires that the momentum transfer in parallel to the surface be small compared with the momentum transfer normal to the surface, i.e., Refs. [28,32],

$$|\boldsymbol{K}' - \boldsymbol{K}| \ll 2k_z, \tag{10}$$

where k_z is the incident wave number in the z direction, $\boldsymbol{K}$ is the incident wave vector in parallel to the surface plane (zero in our simulations), and $\boldsymbol{K}'$ is any intermediate or final wave vector in parallel to the surface plane

which plays a significant role in the scattering process. For a surface area A of atom type X which contains a collection of defects of the same atom type, the angular intensity distribution is given by the function

$$P_{K\to K'} = \frac{1}{A^2}\left|\int \mathrm{d}\boldsymbol{\rho}\, \mathrm{e}^{2\mathrm{i}\eta(\boldsymbol{\rho})+\mathrm{i}\boldsymbol{\rho}\cdot(\boldsymbol{K}'-\boldsymbol{K})}\right|^2, \tag{11}$$

where $\boldsymbol{\rho} = (x, y)$ and $\eta(\boldsymbol{\rho})$ is the scattering phase shift computed for fixed $\boldsymbol{\rho}$, given in the WKB approximation by:

$$\eta(\boldsymbol{\rho}) = \int_{z_t(\boldsymbol{\rho})}^{\infty} \mathrm{d}z \left(\sqrt{k_z^2 - \frac{2mV(\boldsymbol{\rho}, z)}{\hbar^2}} - k_z\right) - k_z\, z_t(\boldsymbol{\rho}), \tag{12}$$

where $z_t(\boldsymbol{\rho})$ is the classical turning point pertaining to the integrand in Eq. (12). Periodic boundary conditions were employed. Condition (10) for the validity of the sudden approximation is expected to break down for systems of high corrugation, and an isolated adsorbate on an otherwise flat surface generally represents, for realistic parameters, a very substantial local corrugation. Nevertheless, previous calculations have shown that the sudden approximation reproduces rather well many features of the scattering from isolated adsorbates [29]. Features for which it breaks down are, e.g. intensity peaks due to double collision events (in which the incoming atom first hits the surface and then the adsorbate or vice versa), which are a particularly sensitive manifestation of a strong corrugation (we note that a double-collision version of the sudden approximation has recently been developed [33]). The sudden approximation is thus useful for the interpretation of these features for which it works, and offers useful insights also at the points where it breaks down. The advantage offered by the simplicity of the sudden expression Eq. (11) is particularly manifest when considering a potential of the form:

$$V(\boldsymbol{r}) = V(z - \xi(\boldsymbol{R})). \tag{13}$$

This form implies that the classical turning surface is a translation of the shape function $\xi(\boldsymbol{R})$ [34]:

$$z_t(\boldsymbol{R}) = \xi(\boldsymbol{R}) + z_0. \tag{14}$$

Here z_0 measures the distance of the repulsive He–surface interaction from some reference plane. The choice of z_0 does not affect the physical observables (i.e., the intensities). z_0 is determined by the incidence energy and angle. Thus Eq. (12) can be rewritten as:

$$\eta(\boldsymbol{R}) = \alpha - k_z(\xi(\boldsymbol{R}) + z_0), \tag{15}$$

where α is a constant independent of $\boldsymbol{R}$. Hence from Eq. (11):

$$P_{K\to K'} = \frac{1}{A^2}\left|\int \mathrm{d}\boldsymbol{R}\, \mathrm{e}^{\mathrm{i}(-2k_z\xi(\boldsymbol{R})+(\boldsymbol{K}'-\boldsymbol{K})\cdot\boldsymbol{R})}\right|^2, \tag{16}$$

thus avoiding the need even for the numerical evaluation of the phase-shift Eq. (12). It should be noted that within the sudden approximation the potential Eq. (13) and a hard-wall potential with the same classical turning surface are essentially equivalent. Under certain assumptions concerning the interaction potential, the angular intensity distribution contains all the information about the scattering process. Indeed, it has been shown by Gerber et al. [35,36] that for an interaction potential of the form $V(\boldsymbol{r}) = V_0(z) + V_1(z)\,Q(x, y)$, if $V_0(z)$ is known, it is possible to determine the form of $V_1(z)$ and $Q(x, y)$ from the angular intensity distribution. This was implemented with good accuracy for a problem where several diffraction peaks only are important, for a crystalline surface. However, in general it is a complicated experimental matter to measure the angular intensity distribution over the entire physical range, and one is usually restricted to several one-dimensional measurements. Interpretation of the angular intensity distribution can very effectively be carried out by analyzing

intensity maxima, which generally fall into three categories: (1) Rainbow peaks [16], related to scattering off inflexion points of the classical turning surface, (2) Fraunhofer peaks [37], caused by interference of waves traveling around a spherical object, and (3) constructive interference (interference) peaks, a consequence of interference of waves scattered from a periodic structure of some sort (which would be classified as Bragg interference for a fully periodic surface). The position of each peak, once identified, contains important structural information about the surface. Our ensuing analysis of the angular intensity distribution will proceed along these lines. Another, particularly simple feature from the experimental point of view, is the attenuation of the specular peak I by a defect. This attenuation is closely related to the cross-section of the defect. The cross-section may be extracted from Eq. (11) via its experimental definition [22]:

$$I = I_0 \, e^{-n \Sigma \theta}, \tag{17}$$

where $I = P_{0\to 0}$, I_0 represents the specular scattering intensity from the corrugated and flat (smooth, defect-free) surfaces respectively, n is the number of defects per unit surface area, and θ their coverage. The parameter Σ in Eq. (17) can be interpreted as the cross-section for scattering by a single defect. When viewed as a function of the incidence energy, I oscillates with a frequency that is characteristic of the height of the defect above the surface. A Fourier analysis of these oscillations reveals the distribution of defect heights, and if performed at a wide enough energy range, will also reveal the z-direction "fine-structure" of these defects. This too will be an approach we shall implement in the next section. A combination of angular intensity distribution and I attenuation analysis proves to be a powerful tool in extracting information about defect structure. This will be developed in the course of our analysis of the results, later in this article.

4. Results and discussion

The results will be outlined by considering separately each of the models described in Section 2. Within each model, we will point out the main physical features present in the scattering calculations, pertinent to the classification of the type of disorder present on the surface. All scattering calculations were performed within the sudden approximation, with the He impinging on Pt(111) at normal incidence. As will be demonstrated in detail in the next sections, there are very dramatic effects in the angular intensity distribution. For the case of the single adsorbed heptamer, nearly all characterizing features of the heptamer's geometrical structure can be discerned in an analysis of the intensity distribution. We are able to determine the symmetry, the linear extents, and the slope and number of inflexion points of the heptameric shape function. Taken together, these define the heptamer almost uniquely. For the case of a distribution of heptamers adsorbed upon the surface, we see significant differences in the scattering results, between the model of translationally random heptamers, and the model of rotationally random heptamers. Both models, in turn, differ most considerably from the case of DLA structures. Furthermore, we are able to quantify the differences among the various cases, relying upon the analysis of the single heptamer. Thus we offer *signatures* of disorder structure based on the analysis of a He scattering experiment. We believe that the great majority of the pertinent features we observe will be experimentally observable. Much like in the case of scattering from ordered surfaces, an analysis of the angular intensity distribution, albeit considerably more complicated, may serve to almost fully classify the type of disorder present on a disordered surface. We proceed to demonstrate how such an analysis may be carried out.

4.1. Physical features in the single heptamer intensity distribution

Fig. 4 shows the results of calculations using the potential discussed in Section 2.1. The collision wavenumber of the impinging He was $k_z = 3.0$ bohr^{-1}. The contour surface shown in Fig. 4 is the full 2D angular intensity distribution, i.e., $P_{\boldsymbol{K}\to\boldsymbol{K}'}$ with the z-axis on a logarithmic scale. What is most striking about Fig. 4 is the unambiguous presence of structure in the intensity distribution: it has a sharp and well-defined angular

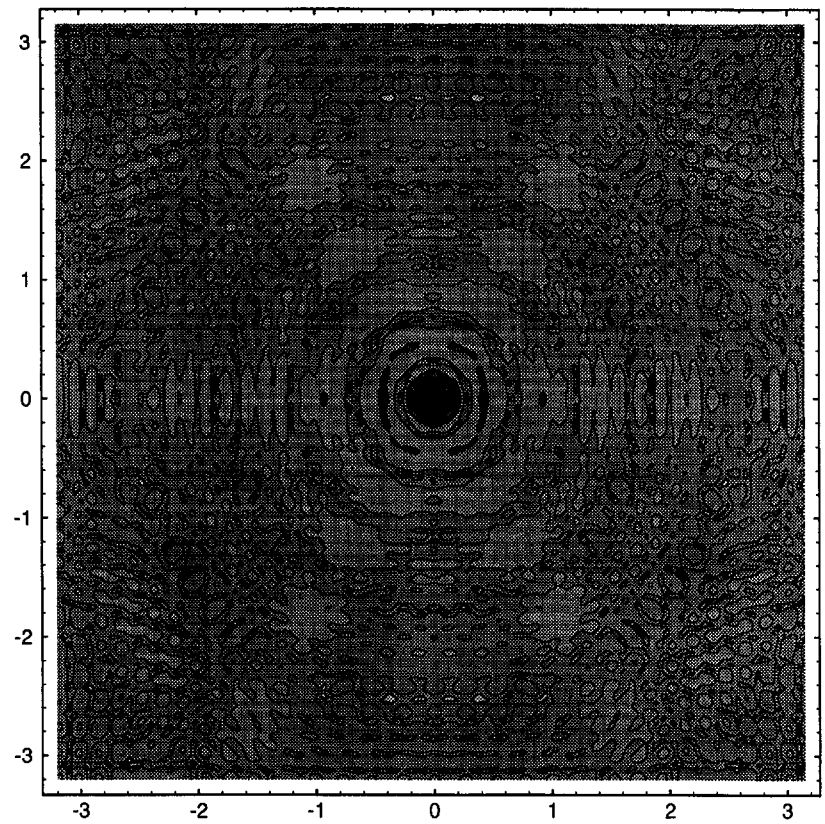

Fig. 4. The full angular intensity distribution for He scattering from a Pt heptamer on a Pt surface, at $k_z = 3.0$ bohr^{-1}. Axes: ΔK_x (horizontal), ΔK_y (vertical). The contours are of the log of the intensities. The six-fold symmetry of the heptamer is clearly maintained in momentum space.

appearance. The structure reflects the six-fold symmetry of the heptamer, as indeed expected from a consideration of Eq. (11). This property is easily shown to hold for other types of symmetry, i.e., the momentum-space view of the cluster via the angular intensity distribution retains the symmetry of the real-space cluster structure. This is a feature which should show up unmistakably in the appropriate experiment, if several on-plane directions are probed. Thus a small cluster on a surface has an experimental signature.

4.1.1. Rainbow, interference and Fraunhofer effects

In this section we will present in some detail an analysis of the major physical features present in the angular intensity distribution. This distribution is however much too detailed to give a full analysis. Such an analysis is definitely desirable to fully characterize the type of disorder present on the surface: in practice the angular intensity distribution contains enough information to leave no ambiguity. It will however be clear from the following, that even a partial analysis may lead one a long way toward an understanding of the disorder one is dealing with. At the end of the section we summarize the main findings.

Fig. 5 shows a section along the ΔK_x axis (at $\Delta K_y = 0$) for scattering at a wave-number of $k_z = 3.0$ bohr^{-1}, with a resolution of 0.05 bohr^{-1} along the ΔK_x axis. The angular intensity distribution in Fig. 5 exhibits, in addition to a large specular peak, also a multitude of other peaks and "hidden" peaks, the pattern being obviously symmetric in the momentum transfer $\Delta K_x = K_x' - K_x$ ($K_x = 0$) direction. In order to interpret the

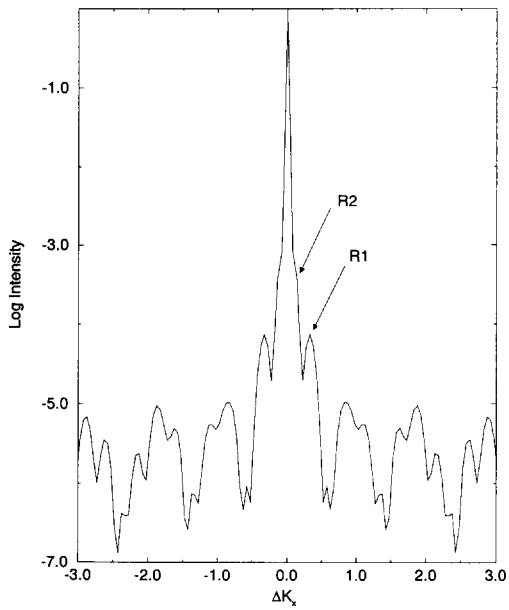

Fig. 5. Log He scattering intensity as a function of momentum transfer in x direction, at $k_z = 3.0$ bohr^{-1}. Positions of rainbow peaks are indicated.

various peaks we proceed along the lines mentioned in the previous section, i.e., we attempt to classify the peaks whenever possible as either rainbows, Fraunhofers or interferences.

Rainbows: The take-home message from the ensuing analysis, is that rainbow peaks appear as a dominant and experimentally observable feature in the angular intensity distribution of He scattered from a single compact cluster, and that their position contains critical information about the surface morphology in the vicinity of the cluster, and about the interaction potential with the He. Measurement of the rainbow peaks alone, is sufficient to calibrate important points in a simple model potential, and is hence a powerful tool in analysis of the surface disorder. Following will be a brief reminder of the origin and physical significance of rainbows (this subject has been treated in much detail elsewhere; see, e.g. Ref. [32]), and a detailed analysis of rainbow-related features in our scattering results.

It is useful to employ a stationary phase, approximate evaluation of the sudden scattering amplitude, as in Ref. [29]. The crude quasi-classical stationary phase limit of Eq. (11) predicts a rainbow whenever the phase-shift has an inflexion point [29]:

$$\eta''(x) = 0. \tag{18}$$

The x_0 satisfying this condition dominates the scattering. In the classical limit this should show up as a singularity in the angular intensity distribution at momentum transfer ΔK_x such that

$$\Delta K_x = -2\,\eta'(x_0), \tag{19}$$

where x_0 is the stationary phase point of the integrand Eq. (11) for momentum transfer ΔK_x. The singularity of the crude classical evaluation is smoothed into a finite peak in the more refined sudden calculation. Fig. 6 shows the phase-shift function $\eta(x)$ at $y = 0$, along with its inflexion points for $k_z = 3.0$ bohr^{-1}. Due to the inversion symmetry of the heptamer about the y–z plane, the inflexion points appear as symmetric pairs along the x-axis.

Each such pair gives rise to corresponding symmetrically located rainbow peaks, as is clear from Eq. (19). The similarity between $\eta(x)$ and the heptamer's isopotential (Fig. 12) is understood from Eq. (14). Based on this similarity, we can identify the physical origin of the rainbow peaks: while it may be difficult to demonstrate this for a general potential (but immediate for, e.g. Eq. (13)), it is clear that in the present case the inflexion points of the phase shift correspond uniquely to those of the turning surface. From Fig. 6 it can be seen that at most four distinct rainbows peaks are expected, one for each inflexion point. The points numbered 1 and 2 are due to the heptamer's top corrugation, number 3 due to its side, and number 4 due to the corrugation induced by the long-range attractive part of the He–Pt interaction at the vicinity of the surface. We expect such inflexion points (and the resulting rainbows) to be widely present for adsorbates on flat surfaces, regardless of the quantitative details of the potentials. In our case, the corrugation associated with point 4 is too small to enable R4 to be discerned from the specular peak. R3 is clearly associated with a double collision in which the He first strikes the heptamer's side and then undergoes a second collision with the flat Pt surface. As mentioned before, such double-collision rainbows cannot be described within the sudden approximation, because it does not include double-collision effects. However, using the quantitative predictions of Eqs. (18) and (19), *we identify the peaks at* $\Delta K_x = \pm 0.33$ *bohr*$^{-1}$ *and the hidden peaks at* $\Delta K_x = \pm 0.13$ *bohr*$^{-1}$ *as R1 and R2, respectively.* The peaks have an intensity of 10^{-4} and 5×10^{-3} respectively with respect to the specular, and should be well within experimental reach (the intensity predictions of the sudden approximation for rainbow peaks are generally in good agreement with the exact quantum-mechanical calculations; see, e.g. Ref. [29]). We did not find a point x_0 that satisfies the rainbow condition Eq. (18), i.e., inflexion points of the phase shift, for the maxima at other ΔK_x values. We found it instructive to compare our results with those obtained by scattering from the same system, at a significantly lower incidence energy. Our motivation was the expectation that at a lower energy, the He probes the Pt system at a more global scale, and is hence more sensitive to the overall structure of the defect and less to local details. This follows also from the reduced penetration depth, resulting in a reduced effective corrugation. The scattering calculations were repeated for the He impinging on the Pt surface at normal incidence, with a wavenumber of $k_z = 2.0$ bohr^{-1}. Fig. 7 shows the same section as Fig. 5 for this energy, with a more than four-fold improved resolution of 0.012 bohr^{-1} (compared to the scattering at $k_z = 3.0$ bohr^{-1}). Fig. 8 shows the corresponding phase-shift at $y = 0$, along with its inflexion points. The inflexion points at the heptamer's top do not persist, as at this low incidence energy, the He particle sees a higher Coulomb barrier in between the top Pt nuclei. Hence it is less effective in penetrating this "soft" region, resulting in the smoothed appearance of the heptamer's top. The absence of inflexion points does not, however, rule out the existence of rainbows: it must be remembered that conditions (18) and (19) follow from a crude stationary-phase analysis and are to be considered merely as sufficient conditions for rainbows. We do however expect a significant reduction in the intensity of the rainbows. Furthermore, analysis of scattering results at $k_z = 4.0$ and 5.0 bohr^{-1} (not presented here) reveals that the position of the rainbows is nearly constant, showing only a slight distancing from the specular peak with increasing kz, as expected from the corresponding increase in corrugation. Returning to Fig. 7 we thus identify the peak at $\Delta K_x = 0.15$ bohr^{-1} as R2. Compared with Fig. 5, its intensity is seen to have indeed decreased by as much as two orders of magnitude. Due to the improved ΔK_x resolution we are now also able to discern the hidden peak at $\Delta K_x = 0.018$ bohr^{-1} as R4, resulting from the long-range attractive part near the edge of the heptamer. R1 is missing, apparently masked by other peaks.

Interference peaks: The origin of these peaks is the constructive interference between He waves scattered from different atoms. On a perfect crystalline surface, these would be referred to as Bragg interference peaks. Here, we expect them to arise from constructive contributions from neighboring Pt adatoms in the heptameric cluster. No contribution can be expected from the surface, as it was treated as completely flat. This is a realistic assumption for Pt(111), which has an extremely smooth surface, whereas the attraction of the heptamer's top electrons to the underlying surface will result in a significant corrugation. Interference peaks are expected at

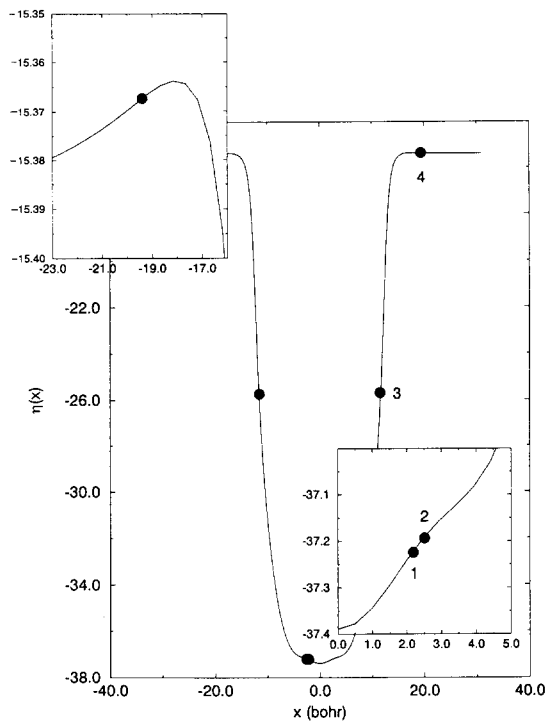

Fig. 6. Phase-shift function $\eta(x)$ as defined in Eq. (12), at $k_z = 3.0$ bohr^{-1}: section along x axis. The inflexion points are indicated.

$\Delta K_x = \frac{2n\pi}{a}$, $a = 5.23$ bohr being the Pt unit cell distance, n an integer, for scattering along the x-direction. However, it turns out that even though these peaks exist, they are of negligible magnitude ($< 10^{-6}$ with respect to the specular) and not within experimental realm. We shall return to this point when we discuss the more realistic system of the next section.

Fraunhofer peaks: Finally we attempted to assign the remaining peaks using the Fraunhofer diffraction model for scattering from a hard hemisphere on a flat, hard surface, given by Lahee et al. [37]. The Fraunhofer diffraction intensities given by this model are:

$$P(\theta) \propto |J_1(d\,k\,\sin(\theta))\,\csc(\theta)|^2\,(1+\cos(\theta))^2\,, \tag{20}$$

where θ is the sum of the incidence and scattering angles (simply the scattering angle in our case), d the hard-sphere radius, k the collision wave-number, and J_1 denotes the Bessel function of 1st order. Given that Eq. (20) is derived under assumptions valid for the scattering of light waves on small obstacles [38], we did not expect it to accurately predict the intensities of the Fraunhofer peaks (see also Ref. [16]). Hence rather than trying to fit Eq. (20) or its parameters to our data, we used a simple prediction resulting from Eq. (20): that the spacing between Fraunhofer peaks as a function of $K_x = k\sin(\theta)$ is very nearly constant. We expect this property of the Fraunhofer model to be more robust than the intensities, as the latter are modified by modulations due to other sources (such as rainbows). While constant spacing cannot be claimed to be unique to the Fraunhofer model, we are not aware of any other relevant model with the same property, which is in addition appealingly simple. Thus we tried to fit a linear regression for the spacings of the remaining peaks. This could be done with a maximum error of 6% per peak and a coefficient of determination $R^2 = 0.995$ (Fig. 9). The constant peak-spacing prediction is expected to persist along the principal axes also, with a more

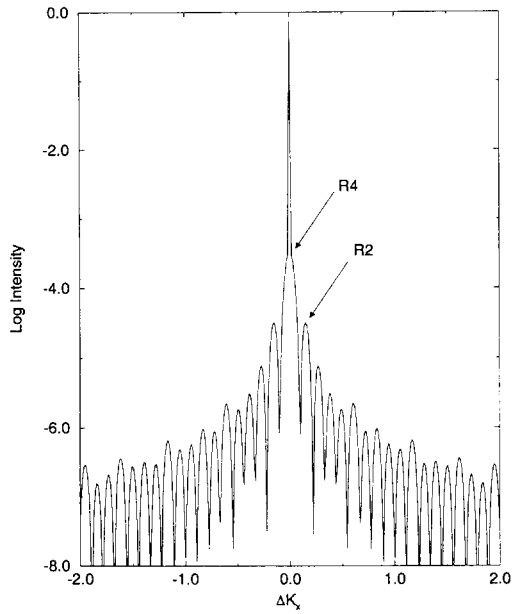

Fig. 7. Log He scattering intensity as a function of momentum transfer in x direction, at $k_z = 2.0$ bohr^{-1}. Positions of rainbow peaks are indicated. A strong Fraunhofer interference pattern is visible.

sophisticated two-parameter model of scattering from a hard ellipsoid replacing the hemisphere. Indeed, we find a value of $\Delta K_y(F)/\Delta K_x(F) = 1.16$ for the ratio of the predicted Fraunhofer peak spacings in the ΔK_y and ΔK_x directions, compared to a geometric ratio of $R_x/R_y = 1/\cos(\pi/6) = 1.15$ between the major and minor axes of the heptamer (the inversion is expected due to the conjugate relationship between real and Fourier space). We thus confidently identify the remaining peaks as Fraunhofer diffraction peaks. Once again, it was instructive to compare these results to the case of a lower incidence energy. Most of the structure in Fig. 7, at $k_z = 2.0$ bohr^{-1}, is in fact due to Fraunhofer peaks. Indeed, the very regular appearance of the non-rainbow peaks and their almost smooth envelope is very reminiscent of a Fraunhofer interference pattern. Relying on the constant spacing property of Eq. (20) again, we were able to fit a linear regression to the peak spacings with a maximum error of 1.3% per peak and a coefficient of determination $R^2 = 0.99995$ (Fig. 9). The dominance and high regularity of the Fraunhofer pattern at this energy is explained by the degree of smoothness of the heptamer itself, in addition to it being a single corrugation on an otherwise flat surface. As we shall see in the next section, this feature breaks down when many adsorbates are present on the surface. The Fraunhofer pattern also obscures any interferences, which were in any case expected to be small due to the low corrugation of the heptamer's top.

4.1.2. The cross-section of a single heptamer

The cross-section, being the simplest parameter to extract experimentally (indeed, the bulk of the experiments done so far in He scattering have been cross-section measurements. See, e.g. Ref. [22]), is probably also the single most descriptive parameter of the surface disorder. As we shall see in this section, the cross-section has an oscillatory behavior in the incidence energy, and there is a mathematical procedure, outlined in appendix A, which enables a determination of the cluster heights distribution from these oscillations alone. However, it should be realized that the necessary large scale variations of the incidence energy are not easily realizable experimentally.

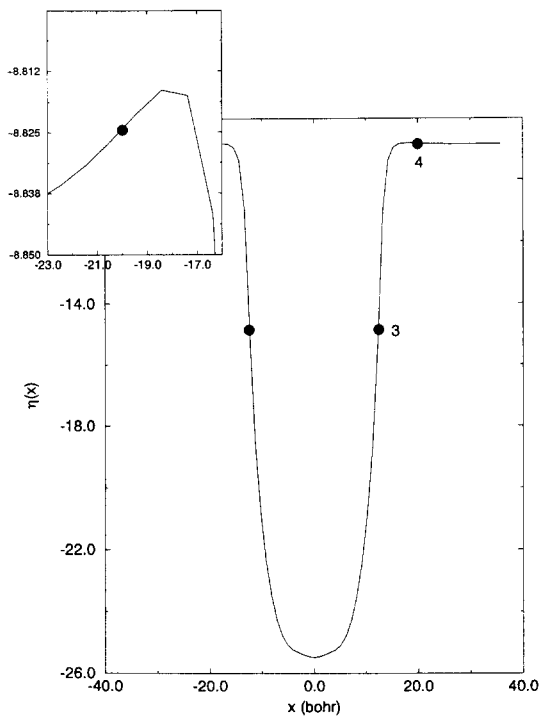

Fig. 8. Phase-shift function $\eta(x)$ at $k_z = 2.0$ bohr^{-1}: section along x axis. The inflexion points are indicated.

Fig. 10 shows the cross-section for He scattering at normal incidence of Pt heptamers at energies corresponding to $k_z = 1, \ldots, 4$ bohr^{-1}. The cross-section was calculated from Eq. (17), which reads:

$$\Sigma = -\frac{\log(\frac{I}{I_0})}{n\theta} \tag{21}$$

when inverted for Σ. In our case $n\theta = 1/(\text{total area})$ (there is one defect – the heptamer – on the entire surface) and $I_0 = 1$ (the defect-free surface is flat). Two main points are worth noting from Fig. 10:

(i) *The value of the cross-section, which lies between 320 and 430* Å^2:
The cross-section of single Pt adatoms on Pt(111) has not been measured yet. We assume it to be similar to that measured for a number of adsorbed molecules and for vacancies, i.e., about 120 Å^2 for a room temperature He beam incident at $\theta_{inc} = 40°$ [22]. This then yields an effective Pt radius of 9 Å, and, using the superposition principle [22] together with a Pt unit cell distance of 2.77 Å, we arrive at a cross-section of about $\pi(2.77+9)^2\cos(40°) = 195$ Å^2 for He scattering off a Pt heptamer at normal incidence. Thus our calculated cross-section is about twice as large as the empirical estimate. This almost certainly reflects the inaccuracy in our value for c_6, as explained in Section 2.1. However, the actual cross-section of a Pt atom on Pt(111) still remains to be measured and it may come out higher than the value employed above. At any rate, our main purpose in this article is to provide qualitative insight into the scattering features. We thus note that it is important to obtain a reliable experimental value for the single adatom cross-section, which once known, can be used to estimate the cluster cross-section. This in turn, can narrow down strongly the number of possible geometric configurations to be considered in attempting to identify the cluster type.

(ii) *The cross-section oscillations*:

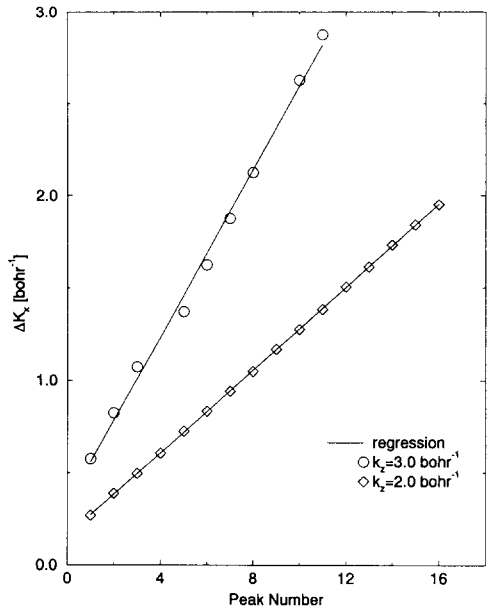

Fig. 9. Constant spacing between peaks in Fraunhofer model: the positions of peaks identified as Fraunhofers in the scattering calculations are displayed as a function of peak number, for two incidence energies. The (nearly) constant spacing between peaks is predicted by Eq. (20).

These arise from interference between waves scattered from the flat part of the Pt surface and the heptamer's top. Clearly the period of oscillations is related to the height difference between the surface and the top of the corrugation. A Fourier analysis of the oscillations in Fig. 10 is shown in Fig. 11, and yields a height difference of about 5.5 bohr. This compares quite well with a direct calculation from the classical turning surface (see Fig. 12), which yields an average height of about 6.5 bohr. In the heptamer case there are effectively two heights to be considered (marked h_1, h_2 in Fig. 12). To see the "fine structure" (h_2) from the cross-section oscillations, clearly a large range of incidence energies must be employed. In the case of the heptamer, our calculations show an unrealistic several hundreds of eV would be required to discern h_2. However, with adsorbates composed of several atom types, or even an adsorbate of different substance than the surface (like in the adsorbate-induced restructuring of surfaces of Cu(110)-(2 × 1) reported by Kern et al. [39]), the situation could be quite different and several experimentally observable heights could exist within one cluster. A theory explaining how to obtain the distribution of cluster heights from the cross-section oscillations is hence desirable, and appendix A provides a detailed calculation of this type in the case of a $V = V(z - \xi(\boldsymbol{R}))$ potential.

4.1.3. Summary of results for a single heptamer

We sum up now briefly the main findings of this section:

(i) Rainbow, Fraunhofer and interference peaks are all expected to be seen with varying intensities in scattering from a heptamer at the same collision conditions (i.e., the same experiment).

(ii) The rainbow peaks due to the heptamer's top corrugation are expected to be the most pronounced feature and to lie closest to the specular. Fraunhofer peaks, probing the size of the adsorbate, will vary in intensity and the first few may be masked by the much stronger rainbows, however they are expected to be found at nearly constant spacing. Interference peaks due to constructive interference between waves scattered from

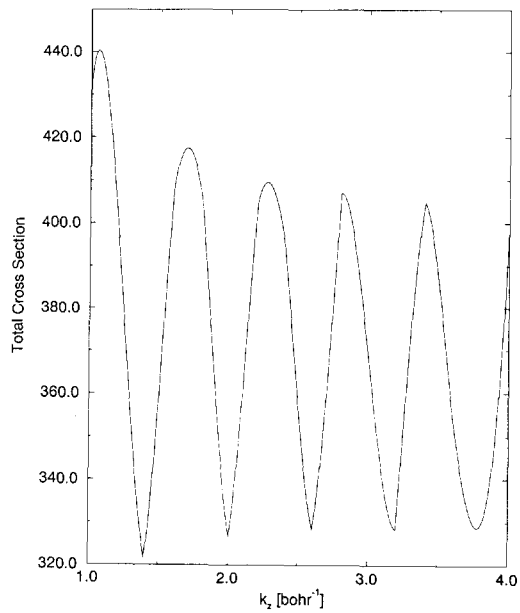

Fig. 10. Total cross-section (in $Å^2$) of the adsorbed heptamer, as a function of He incidence wavenumber k_z ($bohr^{-1}$).

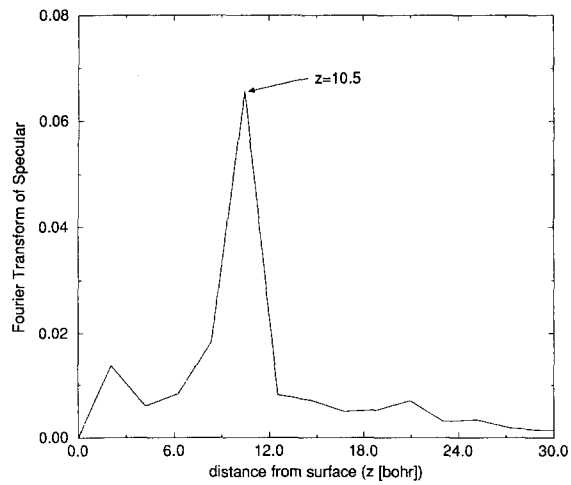

Fig. 11. Fourier transform of the specular intensity versus the height above the surface. The peak at $z \approx 10.5$ bohr corresponds to a distance of $\equiv 5.5$ bohr from the heptamer's top to the surface, as explained in Appendix A.

the heptamer's top atoms may be too weak to be measured experimentally.

(iii) As the incident He's energy is lowered, we expect the angular intensity distribution to become more regular, with the Fraunhofer peaks gradually overtaking the rainbow peaks in dominance. This reflects the prevailing of the small-scale corrugation at high energies, which is smoothed out when the De Broglie wavelength of the incident He becomes more comparable with the heptamer's dimensions at $k_z \leq 1.2$ $bohr^{-1}$.

(iv) The cross-section is a most useful tool in that it is both very simple to obtain experimentally and also provides very important information about the defect's size and topography. The size information can be

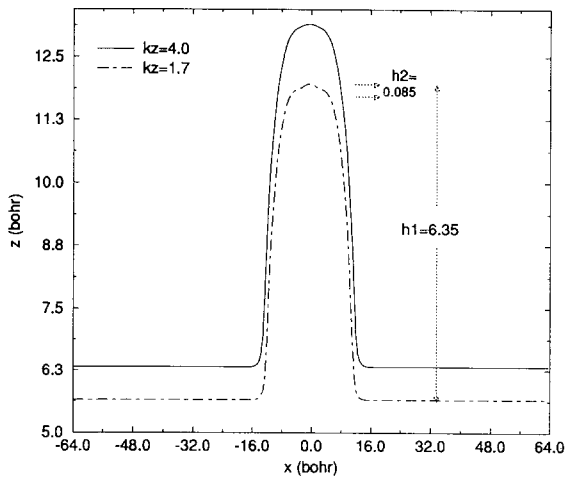

Fig. 12. Heptamer classical turning surface at $y = 0$ for two He incidence wavenumbers: $k_z = 4.0$ bohr^{-1} and $k_z = 1.7$ bohr^{-1}. The two heights relevant to the distribution of surface heights are indicated.

used to narrow down the possible candidates for cluster shapes, and the topography provides an excellent characterization of the defect's appearance.

(v) As each of the scattering features discussed here is sensitive to different aspects of the interaction potential, experiments measuring all these features should provide a nearly complete signature of a heptamer, if present on a surface. This conclusion should hold quite generally for other adsorbate shapes. For example in the heptamer case, the prevailing of Fraunhofer peaks at low incidence energy suggests one is dealing with a nearly hemispherical, i.e., compact object. One may then combine the measured cross-section and the diameter estimated from the Fraunhofer peaks' position to calculate how many Pt atoms participate in a given cluster. The number of observable rainbow peaks gives one a lower bound on the number of distinct inflexion points in the cluster, which can be used to geometrically reconstruct the cluster. The positions of the rainbow peaks tell one about the degree of corrugation of the cluster. An analysis of the cross-section oscillations reveals the number of different heights in the cluster, their values and relative frequency of appearance. Taken together, these data combine to determine the cluster quite fully.

We proceed now to examine the more realistic model of scattering from a collection of randomly adsorbed heptamers.

4.2. *Scattering results from randomly adsorbed heptamers and DLA structures*

In the following sections we analyze in some detail the results for scattering from the randomly adsorbed heptamers and the DLA structures. The main message here, is that structural features persist in the angular intensity pattern of distributions of compact clusters, and can be quantified to extract interesting parameters of the disorder. Very little structure, if any, however, persists in the intensity distribution of DLA, in sharp contrast to the compact cluster case. Thus a scattering experiment can readily distinguish between compact clusters and DLA adsorbed on a surface. We proceed to analyze our results. A summary is presented at the end of the section.

4.2.1. *Translationally random heptamers on Pt(111)*

Fig. 13 shows the results of the scattering calculations from the system described in Section 2.2.1, again

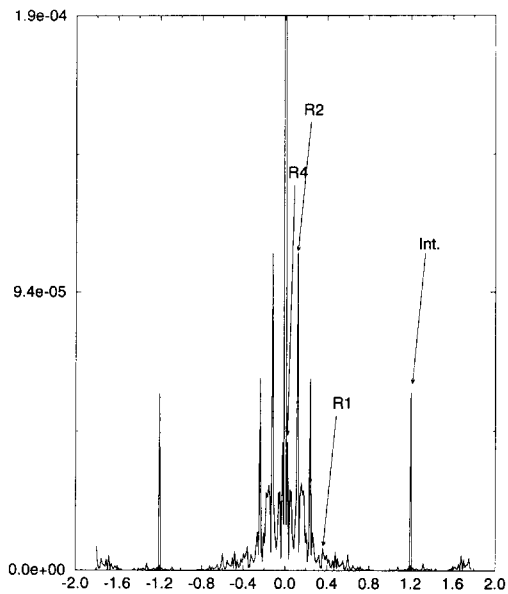

Fig. 13. He scattering intensity distribution from translationally random heptamers, along ΔK_x (bohr^{-1}) axis. He incident at k_z = 2.0 bohr^{-1}. Rainbow (R) and constructive interference (Int.) peaks are indicated.

for k_z = 2.0 bohr^{-1}. There is a rich structure in this angular intensity distribution and we shall not attempt to assign every peak. However, relying on the analysis of the previous sections, we identify rainbow peaks at $\Delta K_x = \pm 0.024$ bohr^{-1} (R4), $\Delta K_x = \pm 0.12$ bohr^{-1} (R2), and $\Delta K_x = \pm 0.36$ bohr^{-1} (R1). These values agree very well with those found in the single heptamer case, and we attribute the small discrepancies chiefly to numerical deviations. The reversal in relative intensities of R4 and R2 (R2 appears more intense now) is believed to be the result of the different role played by the Fraunhofer diffraction pattern in the current system. The optimal conditions for Fraunhofer diffraction are when there is no interference between neighboring clusters, as was certainly the case for the single heptamer. In the present system the average distance between heptamer centers is rather small, giving rise to significant interference between neighboring heptamers. As a consequence the Fraunhofer pattern is strongly attenuated. The increased intensity of R4 in Fig. 7 is hence attributable to an underlying Fraunhofer peak. Considering the shallowness of the attractive well giving rise to R4 (see Figs. 6 and 8, the "normal" state of affairs is restored in Fig. 13, where R2 is the more intense. The attenuation of the Fraunhofer pattern allows for the reappearance of R1, which was missing (masked) in Fig. 7. The strong interference peaks at $\Delta K_x = \pm 1.2$ bohr^{-1} can of course not go unnoticed. Their intensification must be attributed to the constructive contributions of all heptamers, combined with the diminished masking by the Fraunhofer peaks.

4.2.2. Translationally and rotationally random heptamers on Pt(111)

Fig. 14 shows the results of the scattering calculations from the system described in Section 2.2.2, at the same incidence wavenumber of k_z = 2.0 bohr^{-1} as in the previous section. It is most instructive to compare Fig. 14 to 13. Clearly the envelope of the intensity spectrum is much reduced, as expected from the disappearance of most of the constructive contributions when the heptamers assume random orientations. Yet the rainbow peaks persist, albeit at a lower intensity, and we again identify R4 at $\Delta K_x = \pm 0.024$ bohr^{-1}, R2 at $\Delta K_x = \pm 0.12$ bohr^{-1} and R1 at $\Delta K_x = \pm 0.36$ bohr^{-1}. Like the rainbows the interferences at $\Delta K_x = \pm 1.2$ bohr^{-1} are also much weaker, corresponding to the fact that there are now fewer constructive contributions in the original ΔK_x

direction, and most of the intensity is present in other directions.

4.2.3. Scattering pattern for DLA structures

The scattering results from this system, described in Section 2.3 (first model), are presented in Fig. 15. The incident He's wavenumber was once again $k_z = 2.0$ bohr^{-1}. The most prominent feature in Fig. 15 as compared to Figs. 13 and 14 is the almost complete disappearance of structure in the angular intensity distribution. The peaks that can still be discerned are the interferences at $\Delta K_x = \pm 1.2$ bohr^{-1} and a new set at $\Delta K_x = \pm 0.096$

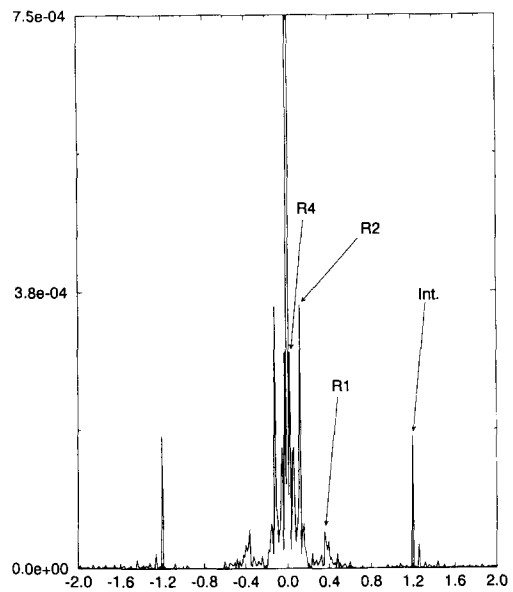

Fig. 14. He scattering intensity distribution from translationally *and* rotationally random heptamers, along ΔK_x (bohr^{-1}) axis. He incident at $k_z = 2.0$ bohr^{-1}.

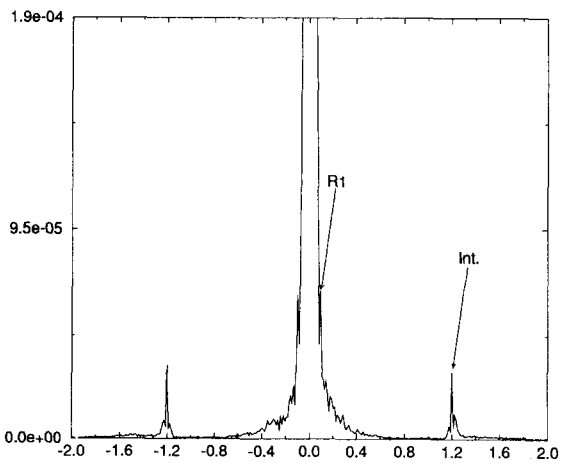

Fig. 15. He scattering intensity distribution from DLA, along ΔK_x (bohr^{-1}) axis. He incident at $k_z = 2.0$ bohr^{-1}.

bohr^{-1}. The existence of the small interference peaks is explained by the hexagonal unit cell structure of the islands. This is of course far from a complete hexagonal surface at the 5% coverage of Fig. 15, but is sufficient to produce some constructive interference between neighboring Pt atoms. The peaks at $\Delta K_x = \pm 0.096$ bohr^{-1} are not at the position of any of the rainbow peaks from the previous two sections, but can still be considered as rainbows, this time an R1 or R2 (they are identical from symmetry considerations except for at the rim of the islands). They arise from the weak corrugation at the top of the monolayer islands. Another dominant feature of Fig. 15 is the broad specular peak. This means that intensity is distributed almost continuously into nearly specular directions. We shall not attempt an analysis of the width of the specular peak and its behavior as a function of ΔK_x here. We shall limit ourselves to mentioning that these features are related to the fractal dimensions of the Pt islands [40]. A detailed examination of this issue in the context of He scattering will be presented in a future article (see also Ref. [14]). Needless to say, no Fraunhofer peaks pattern is observable in Fig. 15.

4.2.4. Summary of results for randomly adsorbed heptamers and DLA structures

To summarize our findings in the last sections:

(i) There is a rich structure of several peaks in the case of He scattering off randomly adsorbed heptamers. Much of this structure persists, albeit at a lower intensity, for the case of randomly rotated heptamers. However, in the case of randomly structured islands, there is nearly no trace of structure in the angular intensity distribution. Thus a powerful preliminary criterion to distinguish structured clusters from randomly shaped ones, is the respective structure of their angular intensity distribution.

(ii) The source of the structure in the angular intensity distribution, in the compact-cluster case, are primarily the rainbow peaks. These are at the same time very robust to perturbations of the structure (e.g. a random rotation of all clusters) and strongly position-related to the fine details of the cluster structure. Thus the rainbow peaks may serve as a crucial component in the identification of surface structure.

(iii) At this relatively low concentration, the Fraunhofer peaks are of secondary importance. They are quite sensitive to adsorbate proximity and shape.

(iv) Interference peaks tend to reflect the underlying surface symmetry as displayed by the adsorbed clusters and are hence not of major help in determining adsorbate structure.

(v) A broad specular peak without much other structure is indicative of randomly shaped islands on the surface.

(vi) The question arises whether the identification of cluster type is still as clear as in the single heptamer case. We believe the answer to be affirmative. The major difference between the single heptamer and randomly adsorbed heptamers cases was the prevailing of Fraunhofer peaks in the former. This resulted from the lack of interference between neighboring clusters in the single heptamer case. This situation can however be experimentally approached by reducing adsorbate concentration. If compact clusters are formed, they will then clearly create a Fraunhofer diffraction pattern. With increasing concentration interference between neighboring clusters will destroy the Fraunhofer pattern, but if the average cross-section remains the same, one may conclude quite safely that compact clusters remain present. If compact clusters do not form at concentrations where there is negligible interference between neighboring clusters, one must resort to relying on rainbows and cross-section analysis alone. However, as discussed in the single heptamer case, this analysis can lead one a long way toward a cluster signature.

5. Concluding remarks

In this study we focused on the utility of TEAS as a tool for learning about surface disorder. More specifically, we sought to demonstrate that the angular intensity distribution of He atoms scattered from adsorbed clusters contains information which can be used to determine most, if not all the characteristics necessary for a signature of a cluster. This determination is based on the identification of rainbow and Fraunhofer peaks in the angular

intensity distribution, and an analysis of cross-section oscillations dependence on incidence energy. All these features, by probing different aspects of the interaction of the adsorbed clusters and the colliding atoms, when taken together, combine to provide an almost complete identification of the cluster. Although our results were obtained for the particular case of heptameric clusters, common physical sense dictates that the qualitative features should persist for other cluster types. That is, as we have demonstrated for heptameric clusters, sharp and well-defined characteristics should be extractable from the angular intensity distribution. This should certainly be so for the case of a single cluster (or a dilute concentration of clusters), and with some more labor for the case of a distribution of clusters. For example, we expect that in the case of a distribution of compact trimers, only one rainbow peak will be seen, the Fraunhofer peak spacing will reflect the structure of the underlying triangular base, and the cross-section will indicate the presence of three atoms. Thus the scattering can serve as a crystallographic tool for disordered surfaces. The major reservation regarding the last statement is, that a distribution of sizes and shapes of clusters, may obscure the otherwise sharp features present in the diffraction spectrum. Viewed from another perspective, as we have shown for the case of translationally random heptamers versus translationally and rotationally random heptamers, versus DLA, inspection of the angular intensity distribution is a means to distinguish one type of disorder from another. We are aware that the effects discussed here are hardly easily detectable. Yet, we have performed our calculations in a realistic energy regime, and by our estimates most of them should be observable with present day techniques and resolutions. On this basis one may anticipate considerable advance in knowledge of compact clusters adsorbed on surfaces and their interaction with incoming atoms, once the pertinent experiments are performed. An issue we have however only scratched the surface of, is that of scattering from DLA. Whereas we have shown that the structure of the angular intensity distribution in this case is substantially different from the compact clusters case, and hence such structures are easily distinguished from compact clusters, it is as of yet an open question what information can be extracted from the angular intensity distribution in this case and how this information could be used to characterize such structures. Work on this issue is in progress and once completed should significantly enhance our ability to understand surface clusters. In light of the very impressive results obtained recently by means of the STM technique (see, e.g. Refs. [41,42]), a few comments on the relative position of the two techniques are in order. In our view, TEAS and STM are really *complementary* techniques, in the sense that STM probes the local structure (several millions of $Å^2$), whereas TEAS probes the global structure. In addition, TEAS is better at probing defects with high mobility, and does not damage the surface. However, there is another significant difference, which is frequently overlooked. This is the fact that STM mostly measures the electronic density near the Fermi level, whereas He scattering is sensitive to the *total* electronic density, via the He–surface interaction potential [43]. Thus although He scattering suffers from the significant disadvantage of displaying the surface in momentum space, whereas STM shows the surface in real space, He scattering is applicable to a much wider range of systems (including liquids [44]). STM, on the other hand, can be applied only to metal surfaces. We hope to have convincingly demonstrated that even in a field in which STM has taken a definite lead, He scattering will have much to offer once the pertinent experiments are performed.

Acknowledgements

This research was supported by the German-Israeli Foundation for Scientific Research (GIF), under grant number I-215-006.5/91 (to R.B.G). Part of this work was carried out with support from the Institute of Surface and Interface Science (ISIS) at UC Irvine. The Fritz Haber Center at the Hebrew University is supported by the Minerva Gesellschaft für die Forschung, Munich, Germany. We are very grateful to Professor G. Comsa, Professor B. Poelsema, Professor I. Steinberger, and Dr. P. Zeppenfeld for many discussions that stimulated much of this work.

Appendix A. Calculation of surface heights distribution from specular peak attenuation

It suffices to measure the intensity of the specular peak over a range of incidence energies to obtain the distribution of surface heights. Consider Eq. (16), which was obtained under the assumption of a potential of the form (Eq. (13)):

$$V(\boldsymbol{r}) = V(z - \xi(\boldsymbol{R})).$$

Assuming a specular collision ($\boldsymbol{K}' = \boldsymbol{K}$), we expand Eq. (16) to obtain:

$$I_0(k_z) \equiv P_{\boldsymbol{K}\to\boldsymbol{K}} = \frac{1}{A^2}\int\int \mathrm{d}\boldsymbol{R}\,\mathrm{d}\boldsymbol{R}'\mathrm{e}^{2\mathrm{i}k_z[\xi(\boldsymbol{R}')-\xi(\boldsymbol{R})]}. \tag{A.1}$$

We know that the cross-section, and hence the specular peak intensity, oscillates with the incidence energy. To see this, we Fourier transform $I_0(k_z)$. Defining first the difference between shape functions:

$$\Theta(\boldsymbol{R},\boldsymbol{R}') = -2[\,\xi(\boldsymbol{R}) - \xi(\boldsymbol{R}')\,], \tag{A.2}$$

the Fourier transform is given by:

$$\begin{aligned}\mathcal{I}(z) = \mathcal{F}[I_0(k_z)] &= \frac{1}{\sqrt{2\pi}A^2}\int\int \mathrm{d}\boldsymbol{R}\,\mathrm{d}\boldsymbol{R}'\int \mathrm{d}k_z\,\mathrm{e}^{\mathrm{i}k_z[z-\Theta(\boldsymbol{R},\boldsymbol{R}')]}\\ &= \frac{\sqrt{2\pi}}{A^2}\int\int \mathrm{d}\boldsymbol{R}\,\mathrm{d}\boldsymbol{R}'\,\delta[\Theta(\boldsymbol{R},\boldsymbol{R}') - z].\end{aligned} \tag{A.3}$$

Eq. (A.3) can in principle be solved for $\mathcal{I}(z)$, given the shape function $\xi(\boldsymbol{R})$. We claim that its normalized value for a given height above the surface z, is the relative frequency of appearance of that height. In other words, $\mathcal{I}(z)$ is the distribution of surface heights. To see this, consider the following example, corresponding to a radically simplified "lego"-model of 3D epitaxial growth. Suppose that atoms can adsorb only along the x-axis, and only one nucleation-site is available. Suppose further that the resulting defect's shape-function is adequately represented by a stacking of rectangles of width w and height h. The situation is represented schematically in Fig. 16. Let the number of atoms making up the base of the defect, i.e., the total number of heights be N. We denote the height at x_j by h_j. Let the number of *distinct* heights be M, i.e., there are M different heights $\{l_i\}_{i=1}^{M}$, each appearing n_i times. Thus:

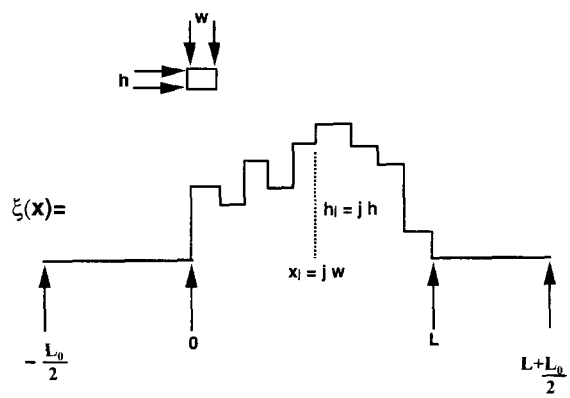

Fig. 16. "Lego" model of 3D epitaxial growth. Schematically drawn is the shape function of the surface with a single defect adsorbed upon it.

$$N = \frac{L}{w} = \sum_{i=1}^{M} n_i. \tag{A.4}$$

Next define a height-function:

$$\Delta_j(x) = \begin{cases} 0 & \text{if } x < jw \text{ or } x > (j+1)w, \\ -2h_j & \text{if } jw \le x \le (j+1)w. \end{cases} \tag{A.5}$$

Using this, we have for given x':

$$\Theta(x - x') = \begin{cases} \Delta_j(x) - \Delta_{j'}(x') & \text{if } 0 \le x, x' \le L, \\ \Delta_j(x) & \text{if } 0 \le x \le L \text{ and } (x' \le 0 \text{ or } x' \ge L), \\ -\Delta_{j'}(x') & \text{if } 0 \le x' \le L \text{ and } (x \le 0 \text{ or } x \ge L), \\ 0 & \text{if } x, x' < 0 \text{ or } x, x' > L. \end{cases} \tag{A.6}$$

Now we can evaluate Eq. (A.3):

$$\int \mathrm{d}x' \int \mathrm{d}x\, \delta[\Theta(x, x') - z] = \int_{-\infty}^{\infty} \mathrm{d}x'\, [I_1 + I_2 + I_3], \tag{A.7}$$

where:

$$I_1 = \int_0^L \mathrm{d}x\, \delta\left[\begin{cases} \Delta_j(x) - \Delta_{j'}(x') - z & \text{if } 0 \le x' \le L \\ \Delta_j(x) - z & \text{if } x' < 0 \text{ or } x' > L \end{cases}\right], \tag{A.8}$$

$$I_2 = \int_{-\infty}^0 \mathrm{d}x\, \delta\left[\begin{cases} -\Delta_{j'}(x') - z & \text{if } 0 \le x' \le L \\ -z & \text{if } x' < 0 \text{ or } x' > L \end{cases}\right], \tag{A.9}$$

$$I_3 = \int_L^{\infty} \mathrm{d}x\, \delta\left[\begin{cases} -\Delta_{j'}(x') - z & \text{if } 0 \le x' \le L \\ -z & \text{if } x' < 0 \text{ or } x' > L \end{cases}\right]. \tag{A.10}$$

Expansion of each term yields:

$$I_1 = \overbrace{\int_0^L \mathrm{d}x' \int_0^L \mathrm{d}x\, \delta[\,\Delta_j(x) - \Delta_{j'}(x') - z\,]}^{\text{III}} + \overbrace{\int_0^L \mathrm{d}x' \int_{-\infty}^0 \mathrm{d}x\, \delta[\,-\Delta_{j'}(x') - z\,]}^{\text{II}} + \overbrace{\int_0^L \mathrm{d}x' \int_L^{\infty} \mathrm{d}x\, \delta[\,-\Delta_{j'}(x') - z\,]}^{\text{II}}, \tag{A.11}$$

$$I_2 = \overbrace{\int_{-\infty}^0 \mathrm{d}x' \int_0^L \mathrm{d}x\, \delta[\,\Delta_j(x) - z\,]}^{\text{II}} + \overbrace{\int_{-\infty}^0 \mathrm{d}x' \int_{-\infty}^0 \mathrm{d}x\, \delta[\,-z\,]}^{\text{I}} + \overbrace{\int_{-\infty}^0 \mathrm{d}x' \int_L^{\infty} \mathrm{d}x\, \delta[\,-z\,]}^{\text{I}}, \tag{A.12}$$

$$I_3 = \overbrace{\int_L^\infty dx' \int_0^L dx\, \delta[\,\Delta_j(x) - z\,]}^{\text{II}} + \overbrace{\int_L^\infty dx' \int_{-\infty}^0 dx\, \delta[\,-z\,]}^{\text{I}} + \overbrace{\int_L^\infty dx' \int_L^\infty dx\, \delta[\,-z\,]}^{\text{I}}. \tag{A.13}$$

It is simple to check that all terms overbraced with the same numeral are indeed equal. Their evaluation yields:

$$\text{I} = (L_0/2)^2\, \delta(z), \tag{A.14}$$

$$\text{II} = \int_L^\infty dx' \sum_{j=0}^{N-1} \int_{jw}^{(j+1)w} dx\, \delta(-2h_j - z) = \frac{L_0}{2}\, w \sum_{j=0}^{N-1} \delta(2h_j + z), \tag{A.15}$$

$$\text{III} = \sum_{j'=0}^{N-1} \sum_{j=0}^{N-1} \int_{j'w}^{(j'+1)w} dx' \int_{jw}^{(j+1)w} dx\, \delta(-2h_j + 2h_{j'} - z) = w^2 \sum_{j'=0}^{N-1} \sum_{j=0}^{N} \delta[2(h_{j'} - h_j) - z], \tag{A.16}$$

where L_0 is the lenght of the defect-free zone.

Collecting all terms and inserting the definition (A.4), we obtain finally the normalized result:

$$\frac{1}{L_0^2}\mathcal{I}(z) = \underbrace{\delta(z)}_{\text{I}'} + \underbrace{\frac{2}{N}\left(\frac{L}{L_0}\right) \sum_{i=1}^{M} n_i\, \delta(z + 2l_i)}_{\text{II}'} + \underbrace{\frac{1}{N^2}\left(\frac{L}{L_0}\right)^2 \sum_{i'=1}^{M} \sum_{i=1}^{M} n_{i'}\, n_i\, \delta[z - 2(l_{i'} - l_i)]}_{\text{III}'}. \tag{A.17}$$

The physical significance of the terms in A.17 is as follows:

(i) I′ represents the contribution of the flat part of the surface: a unit-sized peak at $z = 0$, the reference plane.

(ii) II′ is the most interesting term: it contains a contribution from all heights present on the surface l_i, each weighted by its frequency of appearance n_i. *The sum over these contributions is the sought after distribution of surface heights.* It is scaled as $\frac{1}{N}\frac{L}{L_0}$.

(iii) III′ is a sum of peaks at all possible height *differences*. This information is redundant as it can be extracted from II′. It is scaled as $(\frac{1}{N})^2 (\frac{L}{L_0})^2$ and will therefore be negligible compared with II′.

Eq. (A.17) is a most useful result in our opinion. It shows that a very significant statistical feature of the disorder, the distribution of surface heights, can be extracted with ease from a He scattering experiment. Experimentally, all that needs to be done is to measure the specular scattering at a wide incidence energy range. A Fourier transform will reveal the desired distribution.

The situation for the more realistic situation of defects on a surface (as opposed to a line) is even better: our calculations show that the "noise" term III′ is scaled down by a factor of $(\frac{1}{N})^2 (\frac{L}{L_0})^2$ with respect to the "signal" term II′.

References

[1] S.C. Wang and G. Ehrlich, Surf. Sci. 239 (1990) 301.
[2] G. Rosenfeld, A.F. Becker, B. Poelsema, L.K. Verheij and G. Comsa, Phys. Rev. Lett. 69 (1992) 917.
[3] R. Stumpf and M. Scheffler, Phys. Rev. Lett. 72 (1994) 254.
[4] D.E. Sanders and A.E. DePristo, Surf. Sci. 260 (1992) 116.
[5] T.J. Raeker and A.E. DePristo, Surf. Sci. 248 (1991) 134.
[6] S. Liu, Z. Zhang, G. Comsa and H. Metiu, Phys. Rev. Lett. 71 (1993) 2967.

[7] Z. Zhang and H. Metiu, Surf. Sci. 292 (1993) L781.
[8] B. Poelsema and G. Comsa, Faraday Disc. Chem. Soc. 80 (1985) 16.
[9] B. Poelsema, S.T. de Zwart and G. Comsa, Phys. Rev. Lett. 49 (1982) 578.
[10] B. Poelsema, S.T. de Zwart and G. Comsa, Phys. Rev. Lett. 51 (1983) 522.
[11] B. Poelsema, L.K. Verheij and G. Comsa, Phys. Rev. Lett. 49 (1982) 1731.
[12] H.-J. Ernst, F. Fabre and J. Lapujoulade, Phys. Rev. Lett. 69 (1992) 458.
[13] H.-J. Ernst, F. Fabre and J. Lapujoulade, Phys. Rev. B 46 (1992) 1929.
[14] H.-J. Ernst, F. Fabre, R. Folkerts and J. Lapujoulade, Phys. Rev. Lett. 72 (1994) 112.
[15] H.-J. Ernst, F. Fabre and J. Lapujoulade, Surf. Sci. 275 (1992) L682.
[16] R.B. Gerber, A.T. Yinnon and R. Kosloff, Chem. Phys. Lett. 105 (1984) 523.
[17] A.T. Yinnon, R. Kosloff and R.B. Gerber, Chem. Phys. 87 (1984) 441.
[18] A.T. Yinnon, R. Kosloff and R.B. Gerber, J. Chem. Phys. 88 (1988) 11.
[19] A.T. Yinnon, R. Kosloff, R.B. Gerber, B. Poelsema and G. Comsa, J. Chem. Phys. 88 (1988) 3722.
[20] M. Bott., T. Michely and G. Comsa, Surf. Sci. 272 (1992) 161.
[21] R. Schinke and R.B. Gerber, J. Chem. Phys. 82 (1985) 1567.
[22] B.Poelsema and G. Comsa, in: Vol. 115 of Springer Tracts in Modern Physics, Scattering of Thermal Energy Atoms from Disordered Surfaces (Springer, Berlin, 1989).
[23] J.J. Harris, B.A. Joyce and P.J. Dobson, Surf. Sci. 103 (1981) L90.
[24] H.C. Kang and W.H. Weinberg, Surf. Sci. 299/300 (1994) 755.
[25] H.C. Kang and W.H. Weinberg, Acc. Chem. Res. 25 (1992) 253.
[26] C. Uebing and R. Gomer, J. Chem. Phys. 95 (1991) 7626.
[27] G. Rosenfeld, A.F. Becker, B. Poelsema, L.K Verheij and G. Comsa, in: Surface Disordering: Growth, Roughening and Phase-Transitions, Eds. R. Jullien, J. Kertesz, P. Meakin and D.E. Wolf (Nova Science, Commack, 1993) pp. 97–102.
[28] R.B Gerber, A.T. Yinnon and J.N. Murrel, Chem. Phys. 31 (1978) 1.
[29] A.T. Yinnon, R.B. Gerber, D.K Dacol and H. Rabitz, J. Chem. Phys. 84 (1986) 5955.
[30] D.K Dacol, H. Rabitz and R.B. Gerber, J. Chem. Phys. 86 (1987) 1616.
[31] R.B. Gerber, in: Dynamics of Molecular Processes, Ed. Delgado-Bario (IoP, New York, 1993) p. 299.
[32] R.B. Gerber, Chem. Rev. 87 (1987) 29.
[33] D.A. Hamburger and R.B. Gerber. to be published.
[34] J.I. Gersten, R.B. Gerber, D.K Dacol and H. Rabitz, J. Chem. Phys. 78 (1983) 4277.
[35] R.B. Gerber and A.T. Yinnon, J. Chem. Phys. 73 (1980) 3232.
[36] A.T. Yinnon, E. Kolodney, A. Amirav and R.B. Gerber, Chem. Phys. Lett. 123 (1986) 268.
[37] A.M. Lahee, J.P. Manson, J.P. Toennies and C. Woll, J. Chem. Phys. 86 (1987) 7194.
[38] M. Faubel, J. Chem. Phys. 81 (1984) 5559.
[39] K. Kern, H. Niehus, A. Schatz, P. Zeppenfeld, J. Goerge and G. Comsa, Phys. Rev. Lett. 67 (1991) 855.
[40] P. Pfeifer and M.W. Cole, New J. Chem. 14 (1990) 221.
[41] T. Michely, T. Lund, U. Littmark and G. Comsa, Surf. Sci. 272 (1992) 204.
[42] M.G. Lagally, Phys. Today 46 (1993) 24.
[43] J.K. Nørskov, K.W. Jacobsen, P. Stoltze and L.B. Hansen, Surf. Sci. 283 (1993) 277.
[44] R.B. Gerber, A.T. Yinnon, M. Yanuka and D. Chase, Surf. Sci. 272 (1992) 81.